Published in final edited form as:
Mol Biosyst. 2012 October 30; 8(12): 3305–3313. doi:10.1039/c2mb25341k.

Biochemical and structural analysis of aminoglycoside acetyltransferase Eis from *Anabaena variabilis*†

Rachel E. Pricer[a,b], **Jacob L. Houghton**[a,c], **Keith D. Green**[a], **Abdelrahman S. Mayhoub**[a,‡], and **Sylvie Garneau-Tsodikova**[a,b,c]

Sylvie Garneau-Tsodikova: sylviegt@umich.edu

[a]University of Michigan, Life Sciences Institute, 210 Washtenaw Ave, Ann Arbor, MI 48109, USA

[b]University of Michigan, Chemical Biology Doctoral Program, Ann Arbor, MI 48109, USA

[c]University of Michigan, Department of Medicinal Chemistry in the College of Pharmacy, 210 Washtenaw Ave, Ann Arbor, MI 48109, USA; Fax: +1 734-615-5521; Tel: +1 734-615-2736

Abstract

The *Mycobacterium tuberculosis* enhanced intracellular survival (Eis_*Mtb*) protein is a clinically important aminoglycoside (AG) multi-acetylating enzyme. Eis homologues are found in a variety of mycobacterial and non-mycobacterial species. Variation of the residues lining the AG-binding pocket and positions of the loops bearing these residues in the Eis homologues dictates the substrate specificity and, thus, Eis homologues are Nature-made tools for elucidating principles of AG recognition by Eis. Here, we demonstrate that the Eis from *Anabaena variabilis* (Eis_*Ava*), the first non-mycobacterial Eis homologue reported, is a multi-acetylating AG-acetyltransferase. Eis_*Ava*, Eis from *Mycobacterium tuberculosis* (Eis_*Mtb*), and Eis from *Mycobacterium smegmatis* (Eis_*Msm*) have different structures of their AG-binding pockets. We perform comparative analysis of these differences and investigate how they dictate the substrate and cosubstrate recognition and acetylation of AGs by Eis.

Introduction

Upregulation of the enzyme Eis from *Mycobacterium tuberculosis* (Eis_*Mtb*) has been shown to be responsible for kanamycin A (KAN) resistance in a large fraction of KAN-resistant clinical isolates from tuberculosis patients around the globe.[1,2] We recently reported the unique and unprecedented ability of Eis_*Mtb*[3] and of its homologue from *Mycobacterium smegmatis* (Eis_*Msm*)[4] to multi-acetylate a variety of aminoglycosides (AGs). Even though Eis_*Mtb* and Eis_*Msm* are structurally very similar,[5] we identified differences in the substrate recognition by these two Eis homologues and in their inhibition.[4] Di-acetylation of the rigid fused-ring AGapramycin (APR)was observed with Eis_*Msm*, but APR was found to not be a substrate of Eis_*Mtb*. Moreover, the potency of common inhibitors of these two Eis proteins varied between the two homologues. These data were consistent with structural differences between the AG-binding cavities of the two enzymes.

†Electronic supplementary information (ESI) available: Figures showing the structures of the AGs used in this study, coomassie blue-stained SDS-PAGE of purified Eis_*Ava*, mass spectra of AGs multi-acetylated by Eis_*Ava*, Michealis–Menten plots for the kinetic parameters for the Eis_*Ava* catalyzed acetylation of various AGs, table of proton chemical shift determined for NEA and 1,2′-di-acetyl-NEA along with NMR spectra. See DOI: 10.1039/c2mb25341k

Correspondence to: Sylvie Garneau-Tsodikova, sylviegt@umich.edu.

‡On leave from Faculty of Pharmacy, Al-Azhar University, Cairo, 11884, Egypt.

Due to the rising threat of mycobacterial infection from non-tuberculosis mycobacteria and the ever-growing emergence of resistance to AG antibiotics, it is important to extend the analysis of Eis homologues beyond Eis_*Mtb* and Eis_*Msm* to aid in the understanding of Eis substrate recognition principles across the bacterial kingdom.

As a focus of this study, we chose a putative GCN5-related-*N*-acetyltransferase (GNAT) from the cyanobacterium *Anabaena variabilis* ATCC 29413, (termed Eis_*Ava* herein) structurally similar to Eis_*Mtb*. A crystal structure of Eis_*Ava* was deposited into the Protein Data Bank (PDB) by the Joint Center for Structural Genomics (PDB code: 2OZG). In this work, to gain insight into the structural requirements dictating substrate and cosubstrate profile as well as the inhibition of Eis proteins, we performed structural and biochemical comparative studies of Eis_*Ava* with Eis_*Mtb* and Eis_*Msm*. Cyanobacteria do not cause any clinical infections that are treated with AGs. However, the *A. variabilis* ATCC 29413 strain was isolated from a sewage oxidation pond,[6] and the development of resistance to AGs through water contamination has been previously documented in various bacterial species.[7] Thus, exposure to AGs through sewage waste provides a potential explanation as to why a putative AG-acetylating enzyme, Eis_*Ava*, has arisen in this cyanobacterial strain.

Results and discussion

In silico analysis of Eis homologues across 29 bacterial species

To evaluate the evolutionary relationship among the 3 Eis homologues of interest (Eis_*Ava*, Eis_*Mtb*, and Eis_*Msm*), we first performed a phylogenetic tree analysis using 29 Eis homologue sequences from a variety of mycobacterial and non-mycobacterial species (Fig. 1). In general, the mycobacterial and non-mycobacterial Eis homologues can be divided into two distinct clades, with Eis_*Ava* and Eis_*Mtb* being two of the most evolutionary distinct proteins in this set. Interestingly, the Eis homologue from *Mycobacterium abscessus* (Eis_*Mab*) is clustered with the Eis homologues from the non-mycobacterial clade instead of the expected mycobacterial group. The genetic proximity of Eis_*Ava* to Eis_*Mab* further highlights the importance of studying non-mycobacterial enzymes such as Eis_*Ava* to understand the mycobacterial AG-acetylation resistance mechanisms, due to the current increase in drug-resistant *Mab* infections.[8] In the future, the information learned about Eis_*Ava* could additionally be applied to problematic bacterial species closely related to *Ava* that also contain Eis, such as *Enterococcus faecalis* (*Efa*).

Structural comparison of Eis homologues

Eis_*Ava*, Eis_*Mtb*, and Eis_*Msm* all share a tripartite monomer structure containing N-terminal and central GNAT regions and a similar homo-hexameric organization.[3,5] By performing structure-based sequence alignment of these three Eis homologues, we observed that Eis_*Ava* greatly differs in amino acid composition when compared to Eis_*Mtb* (18% sequence identity) and Eis_*Msm* (19% sequence identity; Fig. 2). In contrast, Eis_*Mtb* and Eis_*Msm* are more similar (53% identical). In all 3 Eis proteins, the key catalytic residue involved in catalysis (Tyr125 in Eis_*Ava*) (Fig. 2, yellow circles/squares) is strictly conserved, and those involved in AcCoA binding (Fig. 2, orange circles/squares) are highly conserved. However, the amino acid residues predicted to bind AGs through site-directed mutagenesis studies of Eis_*Mtb*[3] and structure analysis of Eis_*Mtb* and Eis_*Msm*[4] are highly divergent between Eis_*Ava* and Eis_*Mtb*/Eis_*Msm* (Fig. 2, red squares). Taken together, these observations demonstrate the evolutionary divergence between the Eis proteins from mycobacterial and non-mycobacterial species observed in Fig. 1.

Even though Eis_*Ava* greatly differs in amino acid composition from both Eis_*Mtb* and Eis_*Msm*, its structure is generally very similar to those of Eis_*Mtb* and Eis_*Msm* (Fig. 3A and B). To explore the structural similarities and differences among the 3 studied Eis

proteins and their relationship to function, we compared the structures of their substrate-binding cavities (Fig. 3C–E) and observed striking differences. We previously reported that the AG-binding site of Eis_*Mtb* is divided into two distinct narrow channels (highlighted in green and blue in Fig. 3E), while the AG-binding pocket of Eis_*Msm* consists of one wide and open cavity (Fig. 3D), as a result of the small amino acid side-chains of the residues lining one of the two Eis_*Msm* channels (blue channel of Eis_*Msm*: Ala289, Ala287, Gly266, and Gly401; corresponding residues in Eis_*Mtb*: Gln291, Trp289, Ile268, and Glu401). As a result of the broadening of its AG-binding site relative to that in Eis_*Mtb*, Eis_*Msm* can accommodate the structurally rigid APR AG while Eis_*Mtb* cannot.[4] Interestingly, the substrate-binding cavity of Eis_*Ava* is divided into two distinct channels, as in the case of Eis_*Mtb*, but it differs structurally. As in Eis_*Mtb*, the blue channel of Eis_*Ava* composed of Asp283, Ser281, Lys261, and Phe394 (corresponding residues in Eis_*Mtb*: Gln291, Trp289, Ile268, and Glu401) (Fig. 2, blue circles/squares and Fig. 3C and E) is narrow. However, the green channel of Eis_*Ava* is much larger than that of Eis_*Mtb* and could potentially accept APR as a substrate as does Eis_*Msm*. Different positions of the loop between the α1 and α2-helices and the β13-sheet in Eis_*Ava* and Eis_*Msm* (Fig. 3B) are also in part responsible for the broadening of the substrate-binding cavity of these two Eis homologues relative to that in Eis_*Mtb*.

Multi-acetylation, substrate, and cosubstrate specificity profiles of Eis_*Ava*

We recently reported the substrate and multi-acetylation profiles of Eis_*Mtb* and Eis_*Msm*, demonstrating the unique ability of the Eis enzymes to multi-acetylate many AGs.[3,4] To investigate a potential effect of the broadening of the substrate-binding pocket of Eis_*Ava* on its substrate specificity profile, we monitored the acetylation by Eis_*Ava* of 11 AGs: amikacin (AMK), APR, KAN, neamine (NEA), neomycin B (NEO), netilmicin (NET), paromomycin (PAR), ribostamycin (RIB), sisomicin (SIS), spectinomycin (SPT), and streptomycin (STR) (Table 1; Fig. S1 and S3, ESI[†]), by UV-Vis and mass spectrometry assays. To ensure the validity of the comparisons made in this work, we cloned and overexpressed Eis_*Ava* in an identical fashion to Eis_*Mtb* and Eis_*Msm*, which we previously reported (Fig. S2, ESI[†]). As predicted, based on the structural homology with other Eis proteins, Eis_*Ava* is a functional AG-acetyltransferase. As we previously observed with Eis_*Mtb* and Eis_*Msm*, we found SPT and STR to not be substrates of Eis_*Ava*. By mass spectrometry, we observed that the number of acetylated positions on AMK, NEA, NEO, NET, and RIB by the 3 Eis homologues studied was the same for the 3 enzymes. With other AGs, such as KAN and SIS, we found the number of acetylations with Eis_*Ava* to be less than those observed with Eis_*Mtb* and Eis_*Msm*, which were equal for any given AG. Of particular note is the tri-acetylation of PAR by Eis_*Ava* and Eis_*Msm*, in contrast to only di-acetylation of PAR by Eis_*Mtb*. This result suggests that the broader substrate-binding cavities of Eis_*Ava* (Fig. 3C and F) and Eis_*Msm* (Fig. 3D and G) accommodate the large PAR molecule in more orientations than Eis_*Mtb* does. In addition, we found APR to be mono-acetylated by Eis_*Ava*, which corroborated the previously proposed role of the expanded substrate-binding cavity in binding this rigid extended AG. The presence of two channels (one narrow (blue) and one large (green) in Fig. 3C) in the substrate-binding site of Eis_*Ava versus* a single AG-binding pocket in Eis_*Msm* that is larger than the green channel of Eis_*Ava* (Fig. 3D) could explain the mono-acetylation and di-acetylation of APR observed with Eis_*Ava* and Eis_*Msm*, respectively.

[†]Electronic supplementary information (ESI) available: Figures showing the structures of the AGs used in this study, coomassie blue-stained SDS-PAGE of purified Eis_*Ava*, mass spectra of AGs multi-acetylated by Eis_*Ava*, Michealis–Menten plots for the kinetic parameters for the Eis_*Ava* catalyzed acetylation of various AGs, table of proton chemical shift determined for NEA and 1,2′-di-acetyl-NEA along with NMR spectra. See DOI: 10.1039/c2mb25341k

To explore how APR may be accommodated in the binding pocket of Eis_*Ava* for acetylation, we performed docking of APR to Eis_*Ava* and Eis_*Msm* in complex with AcCoA (Fig. 3I and J). The shorter loop between the α1 and α2-helices of Eis_*Ava* that is responsible for the expansion of the green channel of this enzyme when compared to its counterpart in Eis_*Msm* (Fig. 3B, I, and J) could account for the different conformations adopted by APR in the AG-binding site and the different number of acetylations of APR by these two Eis enzymes, mono- *versus* di-acetylation by Eis_*Ava* and Eis_*Msm*, respectively (Table 1). Taken together, the structural analysis of the substrate-binding cavities of Eis homologues and their multi-acetylation profiles revealed that Eis_*Ava* behaves more similarly to Eis_*Msm* than to Eis_*Mtb*.

In addition to studying the AG substrate promiscuity of Eis_*Ava*, we also investigated its cosubstrate profile. We recently showed that Eis_*Mtb* is limited in its cosubstrates, efficiently accepting only AcCoA and *n*-propionyl-CoA and moderately so crotonyl-CoA and malonyl-CoA for transfer onto a few AGs.[10] We determined that among the 6 acyl-CoA cosubstrates tested with Eis_*Ava* (AcCoA, butyryl-CoA, crotonyl-CoA, malonyl-CoA, myristoyl-CoA, and *n*-propionyl-CoA), only the natural AcCoA cosubstrate and its close structural homologue *n*-propionyl-CoA were accepted by the cyanobacterial Eis.

Steady-state kinetic parameters for Eis_*Ava*

To further understand the action of Eis_*Ava* and the subtleties differentiating the 3 investigated Eis homologues, we performed steady-state kinetic measurements of AG acetylation by Eis_*Ava* and compared the Michaelis–Menten parameters, K_m and k_{cat}, to those of Eis_*Mtb* and Eis_*Msm* (Table 2 and Fig. S4, ESI†). In this study, we determined all kinetic parameters (for Eis_*Ava*, Eis_*Mtb*, and Eis_*Msm*) for 500 μM AcCoA, in a range of 0–2500 μM AG, and 0.25 μM Eis. In a previous report, we determined and compared the K_m and k_{cat} values for Eis_*Mtb* and Eis_*Msm* using 100 μM AcCoA, 0–2500 μM AG, and 0.25 μM Eis.[4] AcCoA was used at a higher concentration in this study to ensure that all enzymes were bound to AcCoA thereby allowing a direct interpretation of kinetics as a property of this holo-Eis. For APR, a substrate of Eis_*Ava* and Eis_*Msm*, but not of Eis_*Mtb*, we found that K_m and k_{cat} values are very similar (337 ± 98 μM and 0.019 ± 0.002 s^{-1} for Eis_*Ava* and of 150 ± 43 μM and 0.019 ± 0.002 s^{-1} for Eis_*Msm*). For KAN and NEO, the K_m and k_{cat} values for acetylation by Eis_*Ava* were also more similar to those of Eis_*Msm* than to those of Eis_*Mtb*. Overall, the kinetic parameters of Eis_*Ava* appear to be most similar to those of Eis_*Msm*, which can be explained by the larger substrate-binding cavities of these two enzymes compared to the divided AG-binding site of Eis_*Mtb*. When determining kinetic parameters by varying AG concentrations at a constant concentration of AcCoA, apparent k_{cat} and K_m are, generally, functions of the concentration of AcCoA and, therefore, they are not intrinsic microscopic mechanistic parameters. To determine the true microscopic turnover rate constant for Eis_*Ava*, we performed three sets of experiments varying the concentration of KAN and keeping the concentration of AcCoA constant at 100, 200, or 500 μM. From these experiments, we obtained k_{cat} of Eis_*Ava* to be 0.24 ± 0.04 s^{-1}, similar to the apparent k_{cat} value measured at [AcCoA] = 0.5 mM. This means that this concentration of AcCoA is saturating in the kinetic sense and, unless binding of an AG very strongly disfavours subsequent binding of AcCoA (an unlikely scenario), the apparent k_{cat} values for the other AGs that are given in Table 2 to a good approximation should represent microscopic k_{cat} values.

Regio-specificity of NEA di-acetylation by Eis_*Ava*

We previously demonstrated that Eis_*Mtb*[3] and Eis_*Msm*[4] sequentially tri-acetylate NEA at the 2′-, 6′-, and 1-position. Seeking a deeper understanding of the differences and similarities between the mycobacterial and non-mycobacterial Eis proteins, we sought to

compare the regio-specificity and order of multi-acetylation of NEA by Eis_*Ava* to those by Eis_*Mtb*/Eis_*Msm*. Interestingly, by thin-layer chromatography (TLC) and NMR spectroscopy (^{1}H, gCOSY, zTOCSY, and gHSQC), we could only observe di-acetylation of NEA by Eis_*Ava* (Fig. 4; Fig. S5–S12 and Table S1, ESI†). Remarkably, we also established that the first position of the NEA scaffold acetylated was the 2′-position, as previously observed with Eis_*Mtb* and Eis_*Msm*, but that the second site modified was the 1-position instead of the expected 6′-position. It is important to note that, as established by mass spectrometry, a third position can be acetylated by Eis_*Ava* on the NEA scaffold. The change in order of the position acetylated by Eis_*Ava* could potentially explain why for this enzyme we did not observe by UV-Vis and mass spectrometry assays a third acetylation, which could proceed at the much slower rate. These data suggest that the order and number of acetylations may vary for each AG based on the Eis homologue utilized. Further studies aimed at establishing the number and positions of acetylation on multiple AGs by a variety of Eis homologues are currently underway in our laboratory.

Inhibition of Eis_*Ava*, Eis_*Msm*, and Eis_*Mtb*

We recently reported the discovery and characterization of Eis_*Mtb* inhibitors,[11] which we also showed in some cases to inhibit Eis_*Msm*.[4] As Eis homologues are found in a variety of bacterial strains (Fig. 1), including emerging resistant species such as *Mab*, the importance of finding Eis inhibitors that efficiently work across various species is increasing with the number of resistant bacterial species that harbour Eis homologues continuously rising. To perform preliminary exploration of the potential of the identified Eis_*Mtb* inhibitors against Eis homologues from various bacterial species, we tested 5 Eis_*Mtb* inhibitors against Eis_*Ava* and Eis_*Msm* (Fig. 5 and Table 3). For chlorhexidine (**1**), the IC_{50} value of 20 ± 7 μM observed for Eis_*Ava* was 107-fold higher than that for Eis_*Mtb* (188 ± 30 nM) and 11-fold higher than that against Eis_*Msm* (1.85 ± 0.39 μM). For compounds **2** and **3**, the IC_{50} values were comparable for both mycobacterial strains. Interestingly, for compound **4**, the IC_{50} value of 455 ± 92 nM observed for Eis_*Msm* was 4.4-fold lower than that for Eis_*Mtb* (2.01 ± 0.12 μM). The poor inhibition of Eis_*Ava* by all 5 inhibitors (IC_{50} values of 20 ± 7 μM for compound **1** and >200 μM for compounds **2–5**) tested could be attributed to the electrostatics of its substrate-binding cavity, which is more hydrophobic (Fig. 3F) than in Eis_*Mtb* (Fig. 3H) and in Eis_*Msm* (Fig. 3G). For example, the hydrophobicMet32 and Pro185 residues of the substrate-binding pocket in Eis_*Ava* replace the structurally homologous negatively charged Asp28 and Asp195 in Eis_*Msm*. Therefore, to assess the utility of discovered Eis_*Mtb* inhibitors on new potential Eis homologues, a thorough analysis of the substrate-binding pocket residues is needed.

Reduced activity of Eis homologues towards 6′-glycinyl-KAN

The development of AGs capable of avoiding acetylation by Eis enzymes could present an alternative strategy to the discovery of Eis inhibitors to combat the Eis resistance problem. We recently reported a simple chemical approach for the production of biologically active 6′-*N*-acylated AG derivatives.[12] To explore the potential of these acylated AGs to evade Eis multi-acetylation, we tested 6′-glycinyl-KAN against Eis_*Ava*, Eis_*Msm*, and Eis_*Mtb* (Fig. 6). We observed that in contrast to KAN that efficiently gets multi-acetylated by all Eis homologues tested (blue, red, and green circles in Fig. 6), 6′-glycinyl-KAN is not a substrate for these enzymes (blue, red, and green triangles in Fig. 6). These data demonstrate the potential of developing novel AG derivatives towards combating AG acetyltransferase enzymes.

Conclusions

In this work, we refined our understanding of the details of the substrate recognition for multi-acetylation of AGs by Eis homologues from mycobacterial and non-mycobacterial species. We also explored the applicability of Eis_*Mtb* inhibitors to the inactivation of Eis homologues from other bacterial species. From these studies we concluded that (i) the substrate-binding cavities of Eis homologues vary greatly even though the overall structures of the enzymes are highly comparable, (ii) Eis_*Ava* behaves more similarly to Eis_*Msm* than to Eis_*Mtb*, (iii) the order of acetylation for a given AG can vary for different Eis homologues, (iv) inhibitors of Eis_*Mtb* could be applied with varying degrees of efficiency against bacterial strains containing Eis homologues, with higher potency against mycobacteria, and (v) glycinylation of the 6′-amine of KAN reduces the activity of Eis homologues. Further studies are underway in our laboratory aimed at establishing the positions acetylated by Eis homologues on a number of AG scaffolds. Structure activity relationship studies towards the development of Eis inhibitors with high potency and broad application are also ongoing.

Experimental

Bacterial strains, plasmids, materials, and instrumentation

Chemically competent *Escherichia coli* TOP10 and BL21 (DE3) strains were purchased from Invitrogen (Carlsbad, CA). *A. variabilis* ATCC 29413 genomic DNA was purchased from the American Type Culture Collection (ATCC). The pET28a plasmid used in this study was purchased from Novagen (Gibbstown, NJ). Primers used for PCR were purchased from Integrated DNA Technologies (Coralville, IA). All reagents and enzymes used for cloning, including restriction enzymes, Phusion DNA polymerase, and T4 DNA ligase, were purchased from New England Biolabs (Ipswich, MA). DNA sequencing was performed at the University ofMichigan DNA Sequencing Core. Dithionitrobenzoic acid (DTNB), AcCoA, acyl-CoAs (butyryl-CoA, crotonyl-CoA, malonyl-CoA, myristoyl-CoA, and *n*-propionyl-CoA), and aminoglycosides (AGs) (AMK, APR, KAN, NEO, RIB, SIS, SPT, and STR; Fig. S1, ESI†) were purchased from Sigma-Aldrich (Milwaukee, WI) and used without further purification. The remaining AGs (NEA, NET, and PAR; Fig. S1, ESI†) were purchased from AK Scientific (Mountain View, CA). Eis_*Mtb* and Eis_*Msm* were purified as previously described using the pEis_*Mtb*–pET28a[3] and pEis_*Msm*–pET28a[4] constructs, respectively. All UV-Vis spectrophotometric assays were performed in 96-well plates (Fisher Scientific; Pittsburg, PA) using a multimode Spectra-Max M5 plate reader. A Shimadzu LCMS-2019EV equipped with a SPD-20AV UV-Vis detector and a LC-20AD liquid chromatograph was used for all liquid chromatography mass spectrometry (LCMS) measurements. The PDB structures 3R1K (Eis_*Mtb*), 3SXN (Eis_*Msm*), and 2OZG (Eis_*Aa*) were analyzed using Coot[13] and PyMOL (The PyMOL Molecular Graphics System, Version 1.4.1, Schrödinger, LLC).

Phylogenetic tree creation for Eis homologues

The amino acid sequences of 29 Eis homologues were retrieved from NCBI through the Geneious Pro 4.8.5 program. The phylogenetic tree (Fig. 1) was built by neighbor-joining using the Geneious Pro 4.8.5 program with the following parameters: Jukes–Cantor genetic distance and the cost matrix Blosum45. The NCBI accession numbers for the Eis homologues were YP_325469 (*Ava*), YP_029001 (*Ban*), NP_814755 (*Efa*), YP_001705255 (*Mab*), CCA55694 (*Sve*), ZP_06590713 (*Sal*), NP_628362 (*Sco*), YP_001855041 (*Krh*), ZP_06804610 (*Bmc*), YP_003645809 (*Tpa*), YP_003272441 (*Gbr*), ZP_06852004 (*Mpa*), ZP_05228133 (*Min*), ZP_05216001 (*Mav*), ZP_09975446 (*Mph*), YP_956800 (*Mva*), YP_004079667 (*Mgi1*), YP_001132138 (*Mgi2*), YP_004522750 (*Msp1*), YP_887817

(*Msm*), YP_001071002 (*Msp2*), YP_639864 (*Msp3*), ZP_04749484 (*Mka*), YP_001852011 (*Mma*), YP_004745879 (*Mca*), YP_978521 (*Mbo*), ZP_07418795 (*Mtb1*), CAB03742 (*Mtb2*), and ZP_06450792 (*Mtb3*).

Preparation of pEis_*Ava*–pET28a overexpression construct

PCR for the amplification of the homologous *eis* gene from *A. variabilis* was performed using Phusion DNA polymerase according to instructions provided by NEB. *A. variabilis* ATCC 29413 (*Ava*) genomic DNA was used as the template for PCR with forward primer 5′-GTGCTTCATATGGTAGAACCAATGAC-3′ and reverse primer 5′-CTATGCCTCGAGTTAAAAGAAATCAATC-3′. The amplified PCR product, *eis_Ava*, was inserted into a linearized pET28a vector between *Nde*I and *Xho*I restriction sites. The plasmid containing *eis_Ava* was transformed into chemically competent *E. coli* TOP10 cell and used to confirm the sequence of the Eis_*Ava* gene (gene locus Ava_4977) (University of Michigan DNA Sequencing Core).

Overproduction and purification of Eis_*Ava* protein

The Eis_*Ava* protein, containing a N-terminal His^6-tag, was overexpressed and purified using the pEis_*Ava*–pET28a overexpression construct as previously reported for its homologue in *Mycobacterium tuberculosis* (Eis_*Mtb*).[3] The Eis_*Ava* protein was dialyzed in Tris–HCl buffer (50 mM, pH 7.5 adjusted at rt), flash frozen in the dialysis buffer containing 10% glycerol, and stored at −80 °C. The protein yield after purification was 1.5 mg L^{-1} of culture (Fig. S2, ESI†).

UV-Vis spectrophotometric assay determination of AG selectivity profile of Eis_*Ava*

The Eis_*Ava* acetyltransferase activity was monitored by using Ellman's method in which the CoA thiol, freed by the Eis_*Ava* catalyzed reaction, is reacted with DTNB to produce an increase in absorbance that can be monitored at 412 nm (ε_{412} = 13 600 M^{-1} cm^{-1}).[14] Reactions (200 μL) containing AG (0.1 mM, 1 eq.), acyl-CoA (0.5 mM, 5 eq.), DTNB (2 mM), and Tris–HCl (50 mM, pH 7.5 adjusted at rt) were initiated by the addition of Eis_*Ava* (0.5 μM) at 25 °C. The reactions were monitored by taking readings every 30 s for 1 h in 96-well plate format.

Determination by mass spectrometry of the number of AG amine functionalities acetylated by Eis_*Ava*

To determine the number of acetylations performed by Eis_*Ava* on each AG substrate, we used LCMS. Reactions (30 μL) containing AG (0.67 mM, 1 eq.), AcCoA (6.7 mM, 10 eq.), Tris–HCl (50 mM, pH 8.0 adjusted at rt), and Eis_*Ava* (10 μM) were run overnight at rt. To prepare samples for the LCMS, ice-cold MeOH (30 μL) was added to the reaction mixture, followed by incubation for 20 min at −20 °C to precipitate the protein. Centrifugation (13 000 rpm, rt, 10 min) was then used to pellet the protein and the supernatant was used for LCMS injection after its dilution in H_2O (10 μL of supernatant into 20 μL of H_2O). The whole sample (30 μL) was injected onto the LCMS, used in positive mode with H_2O (0.1% formic acid). Mass spectra showing the number acetylations on AMK, APR, KAN, NEA, NEO, NET, PAR, RIB, and SIS are presented in Fig. S3 (ESI†). These data are also summarized in Table 1.

Molecular modeling of APR with Eis_*Ava* and Eis_*Msm*

The APR structure was built using the Sybyl-X software and minimized to 0.01 kcal mol^{-1} by the Powell method, using Gasteiger–Hückel charges and the Tripos force field. The coordinates of the Eis_*Ava* and Eis_*Msm* (PDB codes: 2OZG and 3SXN, respectively) were downloaded from the Protein Data Bank website. Except for CoA, the H_2O molecules and

all other substructures were removed from the two proteins. In the structure of Eis_*Ava* (PDB code: 2OZG), the selenium atoms were replaced manually by sulfur. An acetyl group was added to CoA in both Eis_*Ava* and Eis_*Msm*. The surrounding protein residues were then kept frozen and the AcCoA was subjected to energy minimization using the Steepest Descent method. Hydrogen atoms were added and the energy of the Eis_*Ava*–AcCoA and Eis_*Msm*–AcCoA complexes were minimized using the Amber force fields with Amber charges. The energy-optimized APR was docked into the AG-binding site in both Eis_*Ava*–AcCoA and Eis_*Msm*–AcCoA minimized complexes using GOLD.[15] The parameters were set as the default values forGOLD. Themaximum distance between hydrogen bond donors and acceptors for hydrogen bonding was set to 3.5Å. After docking, the first-ranked conformation of APR in both cases was merged into the corresponding APR-free Eis_*Ava*–AcCoA and Eis_*Msm*–AcCoA complexes. The new Eis_*Ava*–APR–AcCoA and Eis_*Msm*–APR–AcCoA complexes were subsequently subjected to energy minimization using the Amber force fields with Amber charges. During the energy minimization, the structure of APR and residues within an 8Å radius was allowed to move. The remaining residues were kept frozen in order to save calculation time. The energy minimization, in both cases, was performed using the Powell method with a 0.05 kcal mol^{-1} energy gradient convergence criterion and a distance dependent dielectric function. The Eis_*Ava*–APR–AcCoA and Eis_*Msm*–APR–AcCoA complexes are depicted in Fig. 3I and J.

Characterization of Eis_*Ava* steady-state kinetic parameters

For several AGs tested in this study (APR, KAN, NEA, NEO, and PAR) the kinetic parameters (K_m and k_{cat}) were determined for acetylation by Eis_*Ava* in reactions (200 μL) with a fixed AcCoA (0.5 mM) concentration. For NEA, NEO, and PAR the AG concentration range used was 0, 20, 50, 100, 250, and 500 μM. Due to their higher K_m values, APR and KAN were tested in a higher concentration range of 0, 50, 250, 500, 1000, and 2000 μM. The reaction mixture containing DTNB (2 mM), Tris–HCl (50 mM, pH 7.5 adjusted at rt), and Eis_*Ava* (0.25 μM) was initiated by the addition of AG. Reactions were monitored by taking readings every 20 s for 20 min at 25 °C. For determination of the K_m and k_{cat} parameters, a non-linear regression fit to the Michaelis–Menten dependence was carried out by using Sigma Plot 11.0 software (Systat Software Inc.; San Jose, CA) (Fig. S4, ESI†; Table 2). The same procedure was used to determine the kinetic parameters (K_m and k_{cat}) reported in Table 2 for Eis_*Mtb* and Eis_*Msm*. To determine the microscopic turnover rate constant for Eis_*Ava*, two additional sets of experiments were performed by keeping the concentration of AcCoA at 0.1 and 0.2 mM while varying the concentration of KAN (0, 50, 250, 500, 1000, and 2000 μM).

Monitoring of NEA acetylation by TLC

The eluent system utilized for all TLCs of NEA reactions was 92.5 : 7.5/MeOH : NH_4OH. The TLCs showing various mono-, and di-acetylated NEA along with their respective R_f values are depicted in Fig. 4. The mono-acetylated standards 2′-, 3-, and 6′-acetyl-NEA were obtained by using AAC(2′)-Ic, AAC(3)-IV, and AAC(6′)-Ie/APH(2″)-Ia, respectively. These enzymes were overexpressed and purified as previously reported.[3,16] The acetylation reactions (30 μL) by these enzymes were run at rt in MES buffer (50 mM, pH 6.0 adjusted at rt) (AAC(3)-IV and AAC(6′)-Ie) or in potassium phosphate buffer (100 mM, pH 7.0 adjusted at rt) (AAC(2′)-Ic) with NEA (5 mM, 1 eq.), AcCoA (25 mM, 5 eq.) and AAC enzyme (10 μM). After overnight incubation at rt, the protein was precipitated by addition of MeOH (30 μL; 20 min, −20 °C). The protein was pelleted by centrifugation (13 000 rpm, rt, 10 min). An aliquot (5 μL) of the supernatant was diluted with MeOH (5 μL) before loading onto SiO_2 TLC plates. The di-acetylation control reactions (30 μL) were carried out in a similar fashion with the addition of the second AAC enzyme (10 μM) and an additional portion of AcCoA (25 mM, 5 eq.) after a 24 h incubation period.

The reactions with Eis_*Ava* (30 μL) were run in Tris–HCl (50 mM, pH 7.5 adjusted at rt) with AcCoA (25 mM, 5 eq.), NEA (5 mM, 1 eq.), and Eis_*Ava* (10 μM). At different time points: 0 (before Eis_*Ava* addition), 5, 10, 30, 120 min, and overnight, aliquots (5 μL) were removed and processed as described above before loading onto SiO_2 TLC plates.

Determination by NMR of NEA amines acetylated by Eis_*Ava*

To determine which two positions of NEA are acetylated by Eis_*Ava*, a reaction was designed for characterization in solution by NMR without the need for purification. A reaction (200 μL) containing NEA (10 mM, 1 eq.), AcCoA (50 mM, 5 eq.), and Eis (10 μM) in Tris–HCl (50 mM, pH 7.5 adjusted at rt) containing 12% D_2O was prepared and allowed to proceed to completion as monitored by TLC. After 24 h, ^1H, gCOSY, zTOCSY, and gHSQC NMR experiments were performed on the reaction solution, applying PURGE solvent suppression to establish the positions of acetylation. LCMS was used to confirm the structure identification. Proton connectivity was assigned using zTOCSY, gCOSY, and gHSQC spectra. Representative spectra for 1,2′-di-acetyl-NEA are provided in Fig. S9–S12 (ESI†).

To establish unambiguously the two acetylated positions on the NEA scaffold, the NMR spectra of 1,2′-di-acetyl-NEA were compared to those of a standard of pure NEA [(10 mM in Tris–HCl (50 mM, pH 7.5 adjusted at rt) containing 12% D_2O], which was prepared identically to the reaction mixture, but omitted AcCoA and Eis_*Ava* (Table S1, ESI†). Representative spectra for the standard reaction solution of NEA in the absence of AcCoA and Eis_*Ava* are provided in Fig. S5–S8 (ESI†).

Inhibition of Eis_*Ava* and Eis_*Msm* by compounds 1–5

IC_{50} values were measured by the UV-Vis assay described above. The reactions (200 μL total) were initiated in several steps. The inhibitors **1–5** (Fig. 5) were dissolved in Tris–HCl (50 mM, pH 8.0 adjusted at rt with 10% DMSO) (100 μL) with a fivefold serial dilution with the highest concentration of inhibitor being 250 μM. A second mixture (50 μL) containing Eis_*Ava* or Eis_*Msm* (2 μM), NEO (400 μM), and Tris–HCl (50 mM, pH 8.0 adjusted at rt) was added to the inhibitor solutions and incubated for 10 min at rt. Reactions were initiated by the addition of a third mixture (50 μL) containing AcCoA (8 mM), DTNB (8 mM), and Tris–HCl (50 mM, pH 8.0 adjusted at rt). The final concentrations of compound **1** ranged from 250 μM to 650 pM. The final concentrations of compounds **2–5** ranged from 200 μM to 102 pM. The assay was run in triplicate and the data were normalized to DMSO control reactions. A Hill plot analysis performed by using Kaleidagraph 4.1 software yielded the IC_{50} values.

UV-Vis spectrophotometric assay determination of Eis_*Ava*, Eis_*Msm*, and Eis_*Mtb* activity against KAN and 6′-glycinyl-KAN

The activity of Eis homologues against KAN and 6′-glycinyl-KAN was tested as described for the determination of the AG selectivity profile of Eis_*Ava* described above.

Supplementary Material

Refer to Web version on PubMed Central for supplementary material.

Acknowledgments

This work was supported by a National Institutes of Health Grant AI090048 (SGT), by Rackham Merit Fellowships from the University of Michigan (REP and JLH), by the NIH Cellular Biotechnology Training Program (CBTP) at the University of Michigan (JLH), by the American Foundation of Pharmaceutical Education Fellowship (AFPE)

(JLH). We thank Dr Oleg V. Tsodikov for critical reading of the manuscript. We also thank Ahmed S. A. Mady for help with generating the phylogenetic tree of Eis homologues.

Notes and references

1. Zaunbrecher MA, Sikes RD Jr, Metchock B, Shinnick TM, Posey JE. Proc Natl Acad Sci U S A. 2009; 106:20004–20009. [PubMed: 19906990]
2. Campbell PJ, Morlock GP, Sikes RD, Dalton TL, Metchock B, Starks AM, Hooks DP, Cowan LS, Plikaytis BB, Posey JE. Antimicrob Agents Chemother. 2011; 55:2032–2041. [PubMed: 21300839]
3. Chen W, Biswas T, Porter VR, Tsodikov OV, Garneau-Tsodikova S. Proc Natl Acad Sci U S A. 2011; 108:9804–9808. [PubMed: 21628583]
4. Chen W, Green KD, Tsodikov OV, Garneau-Tsodikova S. Biochemistry. 2012; 51:4959–4967. [PubMed: 22646013]
5. Kim KH, An DR, Song J, Yoon JY, Kim HS, Yoon HJ, Im HN, Kim J, Kim do J, Lee SJ, Lee HM, Kim HJ, Jo EK, Lee JY, Suh SW. Proc Natl Acad Sci U S A. 2012; 109:7729–7734. [PubMed: 22547814]
6. Tischer RG. Nature. 1965; 205:419–420. [PubMed: 14243447]
7. Rice EW, Messer JW, Johnson CH, Reasoner DJ. Appl Environ Microbiol. 1995; 61:374–376. [PubMed: 7887619]
8. Nessar R, Cambau E, Reyrat JM, Murray A, Gicquel B. J Antimicrob Chemother. 2012; 67:810–818. [PubMed: 22290346]
9. Krissinel E, Henrick K. Acta Crystallogr, Sect D: Biol Crystallogr. 2004; 60:2256–2268. [PubMed: 15572779]
10. Chen W, Green KD, Garneau-Tsodikova S. Antimicrob Agents Chemother. 2012; 56:5831–5838. [PubMed: 22948873]
11. Green KD, Chen W, Garneau-Tsodikova S. ChemMedChem. 2012; 7:73–77. [PubMed: 21898832]
12. Shaul P, Green KD, Rutenberg R, Kramer M, Berkov-Zrihen Y, Breiner-Goldstein E, Garneau-Tsodikova S, Fridman M. Org Biomol Chem. 2011; 9:4057–4063. [PubMed: 21365081]
13. Emsley P, Lohkamp B, Scott WG, Cowtan K. Acta Crystallogr, Sect D: Biol Crystallogr. 2010; 66:486–501. [PubMed: 20383002]
14. Ellman GL. Arch Biochem Biophys. 1958; 74:443–450. [PubMed: 13534673]
15. Verdonk ML, Cole JC, Hartshorn MJ, Murray CW, Taylor RD. Proteins. 2003; 52:609–623. [PubMed: 12910460]
16. Green KD, Chen W, Houghton JL, Fridman M, Garneau-Tsodikova S. ChemBioChem. 2010; 11:119–126. [PubMed: 19899089]

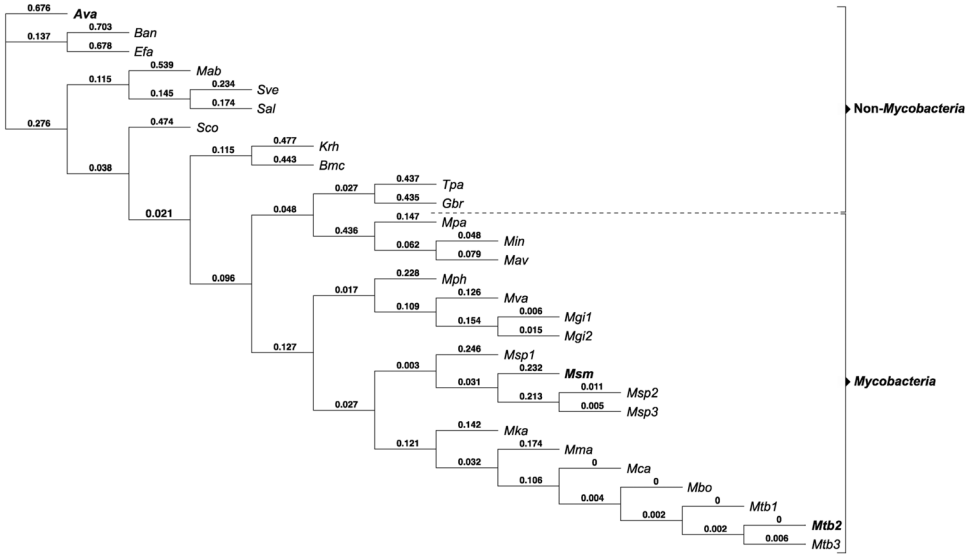

Fig. 1.

Phylogenetic tree analysis of 29 Eis homologues. The numbers are proportional to the evolutionary distance between the branches of the tree. The Eis proteins discussed in this manuscript are in bold. The abbreviated names of the bacterial species correspond to the following: *Anabaena variabilis* ATCC 29413 (***Ava***), *Bacillus anthracis* str. Sterne (*Ban*), *Enterococcus faecalis* V583 (*Efa*), *Mycobacterium abscessus* ATCC 19977 (*Mab*), *Streptomyces venezuelae* ATCC 10712 (*Sve*), *Streptomyces albus* J1074 (*Sal*), *Streptomyces coelicolor* A3(2) (*Sco*), *Kocuria rhizophila* DC2201 (*Krh*), *Brevibacterium mcbrellneri* ATCC 49030 (*Bmc*), *Tsukamurella paurometabola* ATCC 8368 (*Tpa*), *Gordonia bronchialis* DSM 43247 (*Gbr*), *Mycobacterium parascrofulaceum* ATCC BAA-614 (*Mpa*), *Mycobacterium intracellulare* ATCC 13950 (*Min*), *Mycobacterium avium* subsp. *avium* ATCC 25291 (*Mav*), *Mycobacterium phlei* RIVM601174 (*Mph*), *Mycobacterium vanbaalenii* PYR-1 (*Mva*), *Mycobacterium gilvum* Spyr1 (*Mgi1*), *Mycobacterium gilvum* PYR-GCK (*Mgi2*), *Mycobacterium* sp. JDM601 (*Msp1*), *Mycobacterium smegmatis* str. MC2 155 (***Msm***), *Mycobacterium* sp. JLS (*Msp2*), *Mycobacterium* sp. MCS (*Msp3*), *Mycobacterium kansasii* ATCC 12478 (*Mka*), *Mycobacterium marinum* M (*Mma*), *Mycobacterium canettii* CIPT 140010059 (*Mca*), *Mycobacterium bovis* BCG str. Pasteur 1173P2 (*Mbo*), *Mycobacterium tuberculosis* SUMu002 (*Mtb1), Mycobacterium tuberculosis* H37Rv (***Mtb2***), and *Mycobacterium tuberculosis* T17 (*Mtb3*).

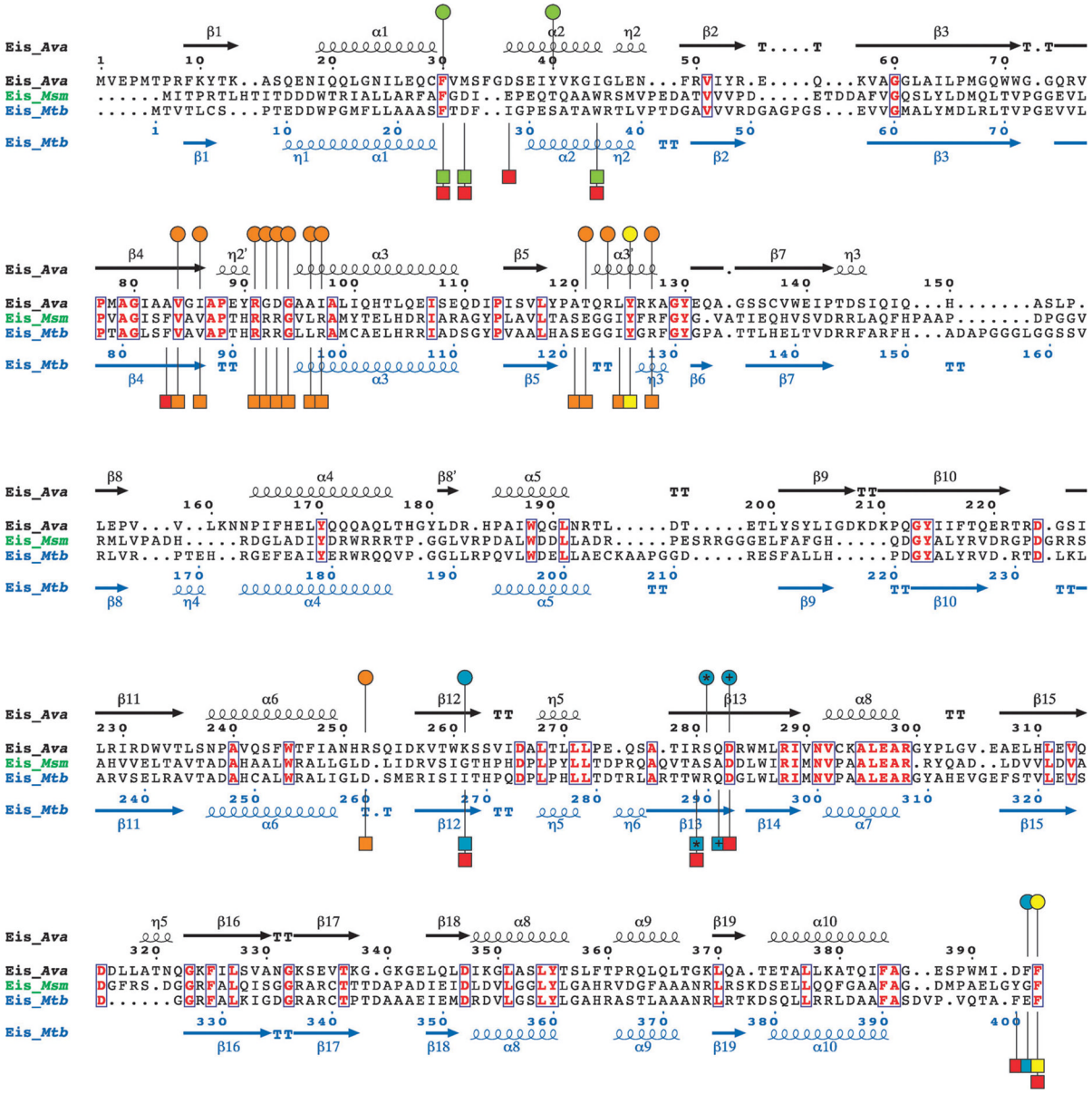

Fig. 2.

Structure-based sequence alignment of Eis_*Ava* from *A. variabilis* ATCC 29413, Eis_*Msm* from *M. smegmatis* str. MC2 155, and Eis_*Mtb* from *M. tuberculosis* H37Rv generated using Secondary-structure matching (SSM).[9] Residues in bold red in blue boxes are conserved between the 3 Eis homologues. The circles above and the squares below the Eis_*Ava* and Eis_*Mtb* sequences, respectively, correspond to important residues in these sequences. Based on structural and mutagenesis studies of Eis_*Mtb*, the residues proposed to be involved in catalysis, in AcCoA binding, and in the formation of the AG-binding pocket are marked by yellow, orange, and red circles/squares, respectively.[3] The AG-binding pocket of Eis_*Mtb* is divided into two channels. Residues lining these two channels are marked by green and turquoise circles/squares. The * and the + symbols indicate residues that structurally aligned when superimposing the crystal structures of Eis_*Ava* and Eis_*Mtb*.

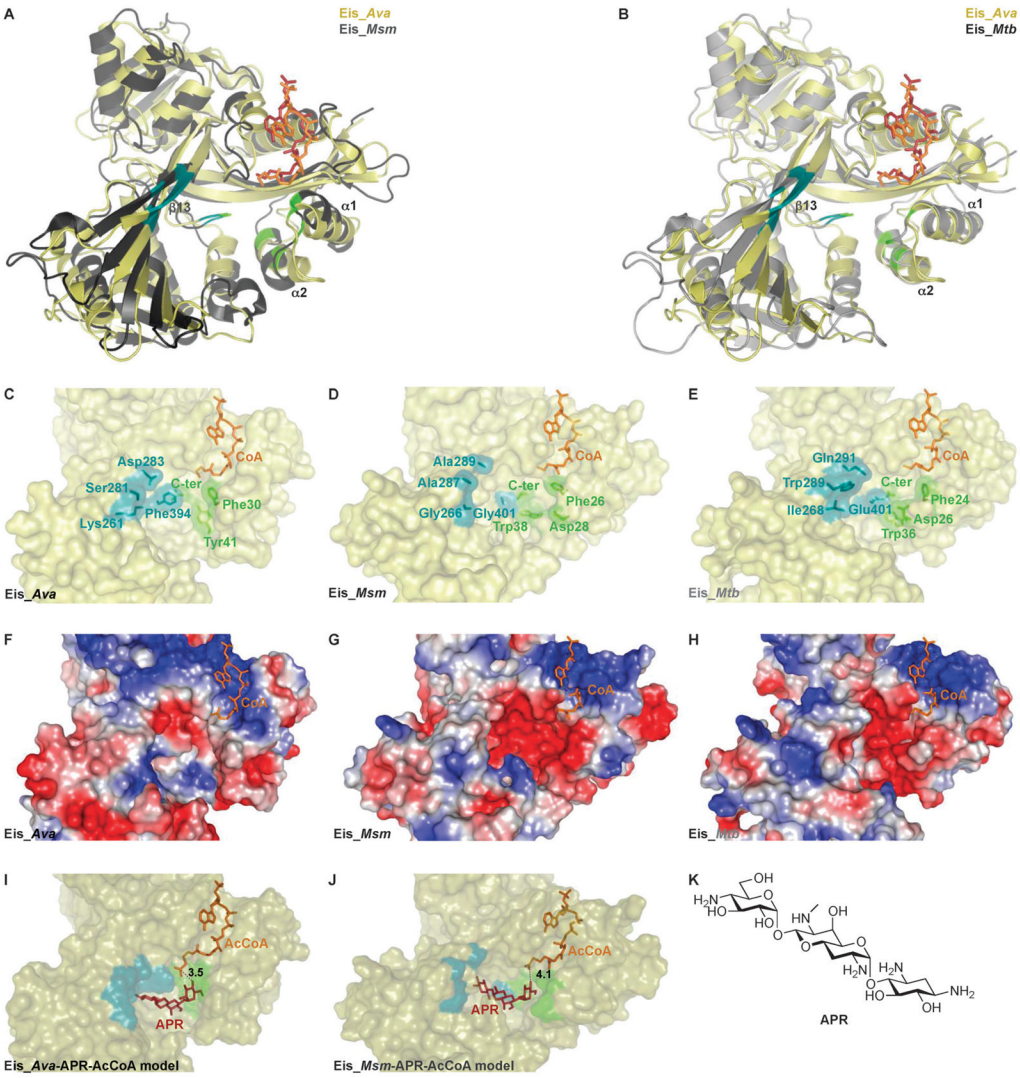

Fig. 3.

Structural comparison of Eis homologues from *Ava*, *Msm*, and *Mtb* as well as molecular models of Eis–APR–AcCoA complexes. (A) Structural alignment of Eis_*Ava* (PDB: 2OZG) with Eis_*Msm* (PDB: 3SXN) (the alignment of one of the monomers of the hexameric structures is shown). (B) Structural alignment of Eis_*Ava* (PDB: 2OZG) with Eis_*Mtb* (PDB: 3R1K) (the alignment of one of the monomers of the hexameric structures is shown). The active site of (C) Eis_*Ava*, (D) Eis_*Msm*, and (E) Eis_*Mtb* with residues lining the two channels (green and blue) of the AG-binding pocket highlighted. Surface representation of the Eis monomer active sites of (F) Eis_*Ava*, (G) Eis_*Msm*, and (H) Eis_*Mtb* colored according to their electrostatic potential, positive in blue, negative in red, and hydrophobic in white. (I) A model of AcCoA and APR bound to Eis_*Ava*. (J) A model of AcCoA and APR bound to Eis_*Msm*. (K) Structure of APR.

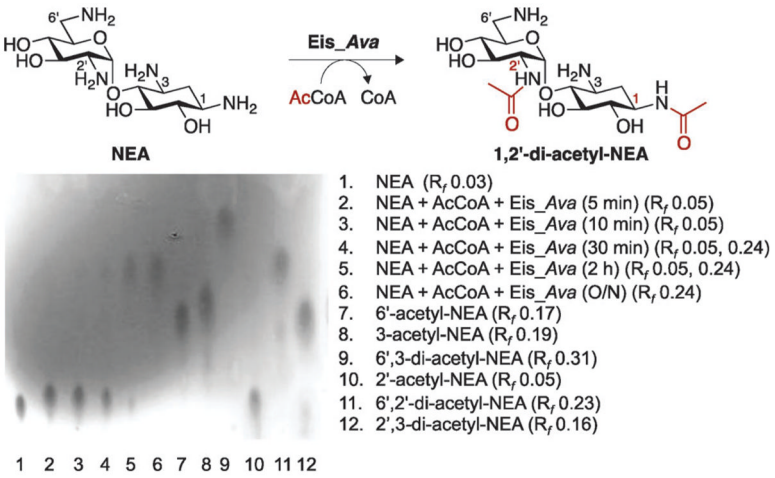

Fig. 4.

Formation of 1,2′-di-acetyl-NEA by Eis_*Ava* monitored by a TLC assay and confirmed by NMR spectroscopy. Lanes 1–6: a time course showing the mono- and di-acetyl-NEA products of the Eis_*Ava* reaction. Lanes 7–12: controls for mono- and di-acetylation of NEA by AAC(2′)-Ic, AAC(3)-IV, and AAC(6′)-Ie used individually or sequentially.

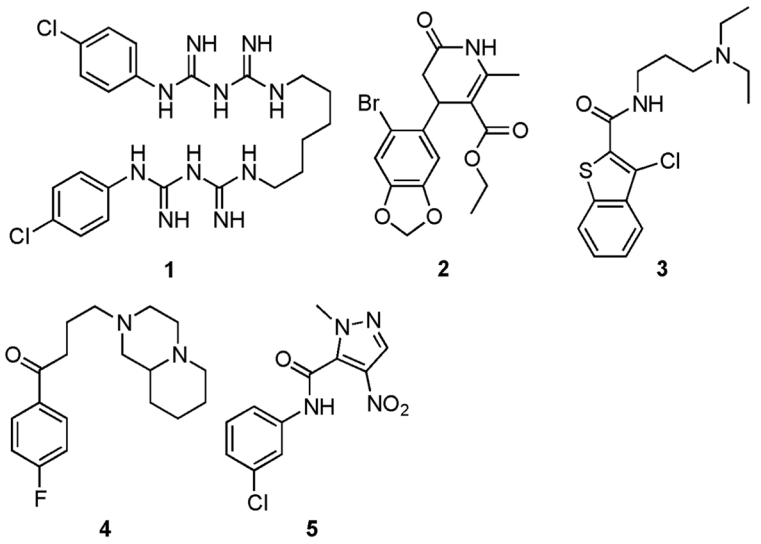

Fig. 5.
Structures of inhibitors tested against Eis_*Ava*, Eis_*Msm*, and Eis_*Mtb*.

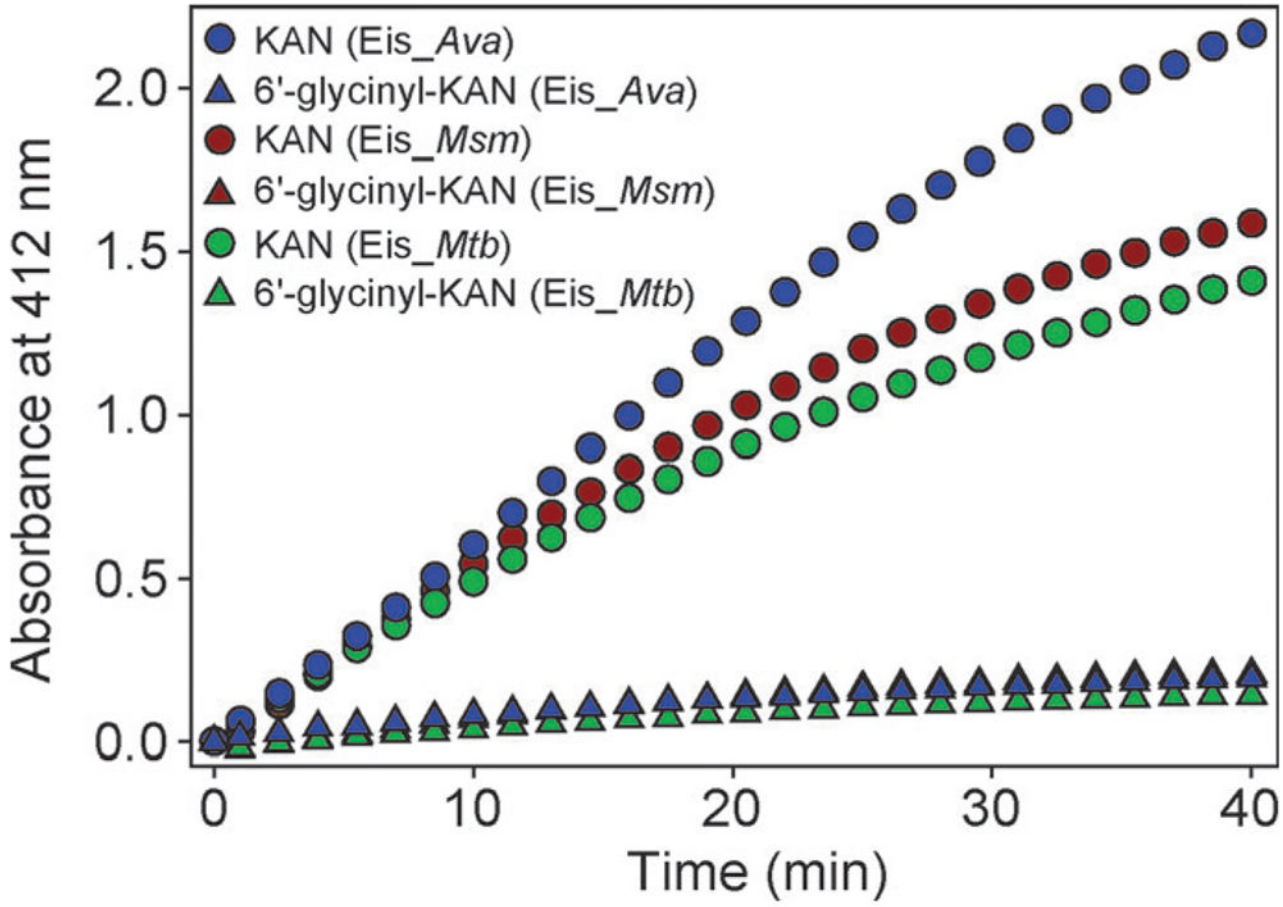

Fig. 6.

UV-Visible spectrum showing the activity of Eis_*Ava* (blue), Eis_*Msm* (red), and Eis_*Mtb* (green) against KAN (circles) and 6′-glycinyl-KAN (triangles). All Eis homologues are almost inactive against 6′-glycinyl-KAN (as a result the red triangles are completely hidden behind the blue triangles).

Table 1

Comparison of number of acetylations of various AGs by Eis homologues from *A. variabilis*, *M. tuberculosis*, and *M. smegmatis*

AG	Eis_*Ava*	Eis_*Mtb*[a]	Eis_*Msm*[b]
AMK	Tri	Tri	Tri
APR	Mono	X[c]	Di
KAN	Mono	Di	Di
NEA	Tri	Tri	Tri
NEO	Tri	Tri	Tri
NET	Di	Di	Di
PAR	Tri	Di	Tri
RIB	Tri	Tri	Tri
SIS	Di	Tri	Tri
SPT	X[c]	X[c]	X[c]
STR	X[c]	X[c]	X[c]

[a] These data were previously reported.[3]

[b] These data were previously reported.[4]

[c] X indicates no observed acetylation.

Table 2

Apparent steady-state kinetic parameters for AG concentration-dependent acetylation by Eis homologues from *A. variabilis*, *M. smegmatis,* and *M. tuberculosis*

Eis_*Ava*			
AG	K_m/μM	k_{cat}/s^{-1}	$k_{cat}/K_m/M^{-1}\ s^{-1}$
APR	337 ± 98	0.019 ± 0.002	57 ± 18
KAN	1002 ± 43	0.205 ± 0.004	205 ± 9
NEA	42 ± 9	0.352 ± 0.021	7413 ± 1938
NEO	101 ± 16	0.106 ± 0.006	1052 ± 184
PAR	237 ± 36	0.183 ± 0.013	773 ± 132
Eis_*Msm*			
APR	150 ± 43	0.019 ± 0.002	127 ± 39
KAN	665 ± 42	0.360 ± 0.010	541 ± 37
NEA	1302 ± 312	0.687 ± 0.083	528 ± 142
NEO	110 ± 14	0.148 ± 0.006	1345 ± 180
PAR	738 ± 158	0.235 ± 0.033	318 ± 82
Eis_*Mtb*			
APR	—[a]	—	—
KAN	330 ± 40	0.526 ± 0.027	1594 ± 250
NEA	1315 ± 492	0.699 ± 0.136	532 ± 224
NEO	122 ± 23	0.610 ± 0.029	5000 ± 972
PAR	110 ± 21	0.136 ± 0.012	1236 ± 260

[a]—Indicates that APR is not a substrate for Eis_*Mtb*.

Table 3

Inhibition of Eis homologues from *A. variabilis*, *M. smegmatis,* and *M. tuberculosis* by compounds **1–5** for NEO acetylation

	IC_{50}/μM		
Compound	**Eis_*Ava***	**Eis_*Msm***	**Eis_*Mtb*[a]**
1	20 ± 7	1.85 ± 0.39	0.188 ± 0.030
2	>200	0.925 ± 0.201	1.09 ± 0.14
3	>200	1.69 ± 0.32	1.24 ± 0.16
4	>200	0.455 ± 0.092	2.01 ± 0.12
5	>200	>200	2.29 ± 0.52

[a]These data were previously reported.[11]